Nigerian Journal of Physics (NJP)
ISSN online: 3027-0936
ISSN print: 1595-0611
DOI: https://doi.org/10.62292/njp.v35(S).2026.757
Volume 35(S), November 2026

Influence of BaO Content on the Physical, Optical, and Radiation Attenuation Properties of Multicomponent Boro-Tellurite Glasses

***Suleman Modu Ngaram[1], Albandari W. Alrowaily[2], Usman Iliyasu[3], Ashok Kumar[4,5], I. Maijawa[1], Mohammed Ibrahim Sayyed[6,7]**

[1]Department of Physics, Federal University, Gashua, Yobe State, Nigeria
[2]Department of Physics, College of Science, Princess Nourah bint Abdulrahman University, P.O. Box 84428, Riyadh, 11671, Saudi Arabia
[3]Department of Physics, Sokoto State University, Sokoto, Nigeria
[4]University College, Benra, Dhuri, Punjab, 148024, India
[5]Department of Physics, Punjabi University, Patiala, Punjab, 147002, India
[6]Department of Physics, Faculty of Science, Isra University, Amman, Jordan
[7]Department of Physics, Dogus University, Dudullu-Ümraniye, Istanbul, 34775, Türkiye

*Corresponding Author's Email: ngaramsuleiman@fugashua.edu.ng Phone No.: +2348027800060

Keywords:
Barium;
Radiation Shielding;
Physical Properties;
Linear Attenuation;
Density

ABSTRACT

Four series of barium-doped boro-tellurite glass samples were fabricated using the conventional melt-quenching technique with nominal compositions (70-x) B_2O_3–$10TeO_2$–$10Bi_2O_3$–5SrO–5ZnO–xBaO, where x = 5, 10, 15, and 20 mol%. The density and molar volume of the fabricated glasses were determined using Archimedes' method. Optical studies observed that the optical band gap increased from 3.016 eV to 3.143 eV and then decreased from 3.055 to 2.847 eV as the BaO concentration increased from 5 to 20 mol%. This increase was attributed to reduced NBO strength within the glass network. We investigated the gamma-ray shielding performance of the fabricated glasses experimentally using a narrow-beam transmission geometry and theoretically using the Phy-X software in the energy range of 0.059-1.333 MeV, both methods show good agreement. The results showed that the highest linear attenuation coefficient (LAC) occurred at 0.059 MeV, increasing from 12.474 cm^{-1} for BT-Ba5 to 18.432 cm^{-1} for BT-Ba20. This enhancement confirms that increasing the BaO concentration significantly improves the gamma-ray attenuation capability of the prepared glasses. Based on the measured LAC values, we evaluated additional shielding parameters, including the half-value layer (HVL), mean free path (MFP), and effective atomic number (Zeff), to provide a comprehensive assessment of radiation-protection performance. Furthermore, we examined the shielding behaviour of the glasses against charged particles (alpha particles and protons). The findings demonstrated that increasing the BaO content enhances the stopping capability of the glasses for alpha particles and protons but reduces the effective removal cross section for fast neutrons.

Submitted: 13/10/2026
Accepted: 18/11/2026
Published: 20/11/2026

INTRODUCTION

The applications of nuclear technology have become increasingly integrated into modern society due to their numerous benefits. They play essential roles in a wide range of fields, including industry, agriculture, medicine, radiology, and the production of clean energy as an alternative (Qazi, 2022; Sonia & Meena, 2024). Despite these significant advantages, exposure to high levels of radiation, particularly ionizing radiation, poses serious health risks to both patients and occupationally exposed workers. Such exposure can lead to severe biological effects, including DNA damage, genetic mutations, cellular dysfunction, and other radiation-induced health disorders (Aniebone & Gafar, 2023; Jahng et al., 2024; Talapko et al., 2024). These biological effects significantly increase the likelihood of developing

cancer (Harrington, 2016; Weeden et al., 2023). Consequently, researchers in radiation protection have focused on developing effective shielding materials to minimise radiation exposure and associated health risks.

Traditionally, concrete and lead (Pb) have been the most widely used materials for radiation shielding (AbuAlRoos et al., 2019; Wu & Wang, 2024). Concrete is considered a conventional and economical shielding material owing to its satisfactory attenuation capability, low cost, widespread availability, and ease of fabrication into various shapes and sizes (Bozkurt et al., 2022). Nevertheless, it has several limitations, including its opacity, which prevents the transmission of visible light, its relatively large thickness requirement for effective shielding, and the degradation of its mechanical properties following prolonged exposure to ionizing radiation (Abdullah et al., 2022; Barbhuiya et al., 2025). Lead, on the other hand, has long been regarded as the benchmark shielding material because of its superior radiation attenuation performance, which is primarily attributed to its high density and high atomic number (Z = 82) (Iliyasu et al., 2025; Kozlovskiy et al., 2023). These characteristics lead to effectively attenuating X-rays and gamma rays over a wide energy range. Despite its excellent shielding efficiency, the use of lead has become increasingly restricted due to its toxicity, environmental hazards, heavy weight, and disposal challenges (Alomairy et al., 2022; Ngaram et al., 2024). Consequently, considerable research efforts have been directed toward developing lead-free, environmentally friendly shielding materials that can provide comparable radiation protection while overcoming the limitations associated with lead (Al-Buriahi et al., 2020; Issa et al., 2022).

Subsequently, glass materials emerged as promising alternatives to conventional opaque radiation shielding materials owing to their unique combination of optical, chemical, and physical properties (Alqahtani et al., 2022; Saudi & Abd-Allah, 2021). Glass offers several advantages, including high transparency to visible light, ease of fabrication, chemical stability, good mechanical strength, and relatively low production cost (Atta et al., 2023; Iliyasu et al., 2025; Ngaram et al., 2024; Ngaram, Hashim, Sanusi, Abdullahi, et al., 2025). Moreover, its radiation shielding performance can be significantly improved through the incorporation of heavy metal oxides (HMOs), which enhance important physical parameters such as density, electron density, and effective atomic number, thereby increasing photon attenuation efficiency (Abdullahi et al., 2024; Alonizan et al., 2023b).

To further improve the shielding effectiveness of glass, numerous studies have incorporated heavy metal oxides, including PbO, Bi_2O_3, WO_3, and other modifying oxides, into the glass network to enhance photon absorption and attenuation (Alomairy et al., 2022; Alzahrani et al., 2022; Wang et al., 2023). However, because of the well-documented toxicity and environmental concerns associated with lead-containing glasses, recent research has increasingly focused on the development of eco-friendly lead-free glass systems (Alonizan et al., 2023b). Among the various heavy metal oxide modifiers, BaO has attracted considerable attention due to its high density, relatively high effective atomic number, high refractive index, excellent infrared transparency, and non-toxic nature (Boonin et al., 2020; Sayyed et al., 2021). Previous studies have consistently reported that increasing the BaO content in the glass matrix improves its density and photon attenuation capability, making BaO-containing glasses promising candidates for radiation shielding applications (Alonizan et al., 2023a).

Boro-tellurite glass systems, which combine the two glass-forming oxides tellurium oxide (TeO_2) and boron oxide (B_2O_3), have demonstrated excellent performance as radiation shielding materials. The strong structural interaction between these network formers promotes the formation of highly interconnected glass networks, resulting in improved structural stability (Mhareb et al., 2025; Ngaram, Hashim, Sanusi, Abdullahi, et al., 2025). Furthermore, by optimizing the ratio of the glass-forming oxides, the hygroscopic nature of the glass can be reduced while enhancing its refractive index and radiation shielding performance (Kozlovskiy et al., 2021). These favorable characteristics make boro-tellurite glasses attractive candidates for transparent radiation shielding applications, as evidenced by previously reported systems such as $SrO–B_2O_3–TeO_2$ (Aloraini et al., 2021) and Dy^{3+}-doped $ZnO–B_2O_3–TeO_2$ (Sathiyapriya et al., 2019).

The incorporation of strontium oxide (SrO) into boro-tellurite glass increases its density, thereby enhancing its radiation shielding performance (Aloraini et al., 2021). The addition of bismuth oxide (Bi_2O_3) further increases the glass's density, thereby improving its suitability for radiation shielding applications in nuclear facilities and medical equipment (Bakri et al., 2024). The incorporation of zinc oxide (ZnO) helps optimize the glass-forming ability and enhance the non-crystalline phase in a boro-tellurite glass network (Alomairy et al., 2022). Several attenuation-related parameters, including the linear attenuation coefficient, mass attenuation coefficient, half-value layer (HVL), mean free path (MFP), radiation protection efficiency (RPE), and effective atomic number (Z_{eff}), are commonly evaluated to assess the radiation shielding performance of materials intended for X-ray and gamma-ray protection. Among these, the effective atomic number is particularly important for heterogeneous materials such as glass, as it provides insight into their photon interaction characteristics. Current research is increasingly focused on developing lead-free glass shielding materials,

emphasizing environmentally friendly alternatives to conventional lead-based radiation shields.

The present research involves the synthesis of glass systems that consist of four sets of glasses prepared based on the composition (70-x) B_2O_3+10TeO_2+10Bi_2O_3+5$SrCO_3$+5ZnO+x$BaCO_3$ (where x = 5, 10, 15, and 20 mol%). The physical properties of the prepared glasses were examined using the Archimedes method, with toluene as the standard liquid, and measurements were performed at ambient temperature. Furthermore, an experimental setup using a narrow-beam transmission geometry and the Phy-X software was employed in the energy range of 0.059-1.333 MeV to evaluate the X-/gamma-ray shielding performance of the prepared glasses. The study deliberately compares the measured parameters from model predictions and identifies the calculations that require theoretical validation.

MATERIAL AND METHODS

Experimental Procedure

Synthesis of Ba-activated boro-tellurite glasses

Four glass samples with the nominal composition $(70-x)B_2O_3$–10TeO_2–10Bi_2O_3–5SrO–5ZnO–xBaO, where x = 5, 10, 15, and 20 mol%, were prepared using the conventional melt-quenching technique. The prepared samples were designated BT-Ba5, BT-Ba10, BT-Ba15, and BT-Ba20, corresponding to $BaCO_3$ concentrations of 5, 10, 15, and 20 mol%, respectively. High-purity (Sigma-Aldrich, 99% purity) precursor powders of B_2O_3, TeO_2, Bi_2O_3, $SrCO_3$, ZnO, and $BaCO_3$ were accurately weighed according to the desired compositions and thoroughly mixed to ensure compositional homogeneity. The homogeneous batches of 20 g were transferred into an alumina crucible and melted at 1100 °C for 30 min. The molten glass was then poured into a preheated stainless-steel mold to produce disc-shaped glass samples. Immediately after quenching, the samples were transferred to a muffle furnace maintained at 400 °C for annealing for 60 min to relieve internal stress, after which they were allowed to cool gradually to room temperature. Cutting and polishing devices (Metkon Micracut 151 and Metkon Forcipol 1V Grinder-Polisher) were used to produce cylindrical-shaped glasses with a thickness of about 2 mm. The radiation shielding performance of the prepared glass samples was experimentally investigated using a narrow-beam transmission geometry in the energy range of 0.059-1.333 MeV at the Radiation Laboratory, Universiti Teknologi Malaysia (UTM). This configuration minimises scattered radiation, ensuring accurate determination of the primary gamma-ray attenuation characteristics of the investigated glass samples. The experimental arrangement consisted of a radionuclide point source, a detector, a lead (Pb) collimator, and the glass samples, which served as absorbing materials. We used Phy-X/PSD to theoretically evaluate the radiation-attenuation properties of the investigated glasses over an energy range of 0.015–15 MeV. The software provides estimates of several important shielding parameters, including the half-value layer (HVL), tenth-value layer (TVL), effective atomic number (Z_{eff}), mean free path (MFP), radiation protection efficiency (RPE), energy absorption buildup factor (EABF), exposure buildup factor (EBF), and fast neutron removal cross-section (FNRCS). The variation in glass density as a function of barium oxide concentration was evaluated by the Archimedes technique (see equation 1) using toluene (ρ_T = 0.8669 g cm^{-3}) as the immersion medium, with all measurements carried out under ambient conditions using a KERN brand ABT 100-5 m model analytical balance with a sensitivity of 0.00001 g. The density of each glass sample was measured three times to reduce error.

$$\rho_{glass} = \frac{W_a}{W_a - W_T} \text{ x } \rho_T \qquad (1)$$

where W_a is the weight of the glass sample in air, W_T is the weight of the glass sample when immersed in toluene liquid, and ρ_T is the density of toluene liquid (0.8669 g/cm^3 at room temperature). The molar volume of the prepared glasses has been evaluated using the following equation:

$$V_m = \frac{M}{\rho} \qquad (2)$$

where M is the average molecular weight of the samples, and ρ is the density of the glass samples. The oxygen packing density (OPD), oxygen molar volume (OMV), polaron radius, ion concentration, inter-nuclear distance and field strength were evaluated using equations elsewhere (Ardiansyah et al., 2023) (see Table 2), which were based on elemental composition data, density changes (ρ) and molar volume. Accordingly, the refractive index of the prepared glass samples was determined using Eq. (3) (Dimitrov & Komatsu, 2010).

$$\frac{n^2-1}{n^2+1} = 1 - \sqrt{\frac{E_{opt}}{20}} \qquad (3)$$

where E_{opt} represents the optical energy band gap of the glasses.

Other refractive-index-dependent optical parameters, such as the dielectric constant, can subsequently be determined using Eq. (4) (I. Usman et al., 2023).

$$\varepsilon = n^2 \qquad (4)$$

where ε is the dielectric constant.

Furthermore, the molar refraction of the prepared glass samples was calculated using the Lorentz–Lorenz relation given in Eq. (5) (Ngaram et al., 2024).

$$R_M = \left[\frac{n^2+1}{n^2+2}\right] V_m \qquad (5)$$

where V_m, R_m and n are the molar volume, molar refraction, and refractive index, respectively.

The UV–Vis–NIR absorption spectra of the transparent glass samples were recorded using a Shimadzu UV-

3600Plus spectrophotometer over the 200–2000 nm wavelength range. The resulting absorption data were used to determine the absorption coefficient and optical band gap of the glasses. The absorption coefficient $\alpha(v)$ was calculated using Eq. (6) (Alazoumi et al., 2018; A. Usman et al., 2018).

$$\alpha(v) = \frac{2.303A}{d} \quad (6)$$

where A is the absorbance, and d is the thickness of the glass sample. Then, the optical bandgap (E_{opt}) is determined through Eqn. (7) (Alazoumi et al., 2018; A. Usman et al., 2018).

$$\alpha(v) = B\left(\frac{hv - E_{opt}}{hv}\right)^m \quad (7)$$

where E_{opt} denotes the optical band gap obtained from Eq. (7), with m = 2 and m = 1/2 corresponding to direct and indirect electronic transitions, respectively. B is a proportionality constant associated with the band-tail characteristics, while m determining the nature of the electronic transition. For direct-allowed, indirect-allowed, direct-forbidden, and indirect-forbidden transitions, the exponent $n$takes values of 1/2, 2, 3/2, and 3, respectively. In indirect transitions, phonon interactions are required to conserve momentum because the electron wave vector changes during the optical transition. Accordingly, for an indirect allowed transition, $(\alpha hv)^{1/2}$exhibits a linear dependence on photon energy. The optical band gap, E_{opt}, is determined by extrapolating the linear portion of this relationship to the energy axis, where $(\alpha hv)^{1/2} = 0$.

Radiation attenuation performance

The linear attenuation coefficient (LAC) is a fundamental radiation shielding parameter that quantifies the capacity of a material to attenuate incident ionizing radiation. For a given glass sample, the LAC can be determined experimentally using the Beer–Lambert law and by utilizing Phy-X software, as expressed in Eqn. 8 (Alzahrani et al., 2022; Ngaram, et al., 2025).

$$I = I_0\, e^{-\mu k} \quad (8)$$

where I represent the intensity of gamma-ray photons transmitted through the glass sample, I_0 denotes the initial intensity of the incident gamma-ray photons, μ is the linear attenuation coefficient, and $k$corresponds to the thickness of the glass samples. Half-value layer (HVL) is defined as the thickness of the investigated glass sample required to reduce the intensity of the incident gamma-ray photons to 50% of their original value. The HVL was calculated using Eqn. (9) (Ngaram, et al., 2025).

$$\text{HVL} = \frac{\ln 2}{\mu glass} \approx \frac{0.693}{\mu} \quad (9)$$

Another important radiation shielding parameter used to characterize multi-element materials in terms of an equivalent atomic number is the effective atomic number (Z_{eff}). For the investigated glass samples, the Z_{eff} values were evaluated using Eqn. (10) (Mhareb et al., 2020).

$$Z_{eff} = \frac{\sigma_a}{\sigma_{el}} \quad (10)$$

where σ_a and σ_{el} are atomic and electronic cross-sections, respectively, while the atomic cross-section can be evaluated via Eqn. 11 (Knoll, 2010).

$$\sigma_a = \frac{\mu_m}{N_A \sum_i \frac{w_i}{A_i}} \quad (11)$$

where A_i and N_A are the atomic weights of the i^{th} element in the material's composition and Avogadro's number, respectively; the electronic cross-section is determined using Eqn. 12 (Knoll, 2010).

$$\sigma_{el} = \frac{1}{N_A}\sum_i \frac{f_i A_i}{Z_i}(\mu_i) \quad (12)$$

where f_i is the fraction of atoms of element i relative to the total number of atoms of all elements, and Z_i is the atomic number of the ith element.

RESULTS AND DISCUSSION

Physical properties

The physical properties of the fabricated boro-tellurite glasses demonstrated a systematic increase in density and molar volume with increasing BaO concentration, accompanied by a decrease in B_2O_3, providing structural modifications within the glass network. The increased density from 4.028 g cm^{-3} (BT-Ba5) to 4.813 g cm^{-3} (BT-Ba20) can be attributed to the higher atomic mass of Ba^{2+} replacing the network former B^{3+} in B_2O_3, acting as a network modifier while increasing the total mass per unit volume of the glass. The presence of heavier metals (Bi_2O_3 and TeO_2) further elevated the glass density with a denser network structure and the average atomic weight of the glass. These resulted from the larger ionic radius 1.35 Å of Ba^{2+} replacing B^{3+} (0.23 Å), causing glass expansion from 32.840 (BT-Ba5) to 37.063 cm^{3}mol^{-1} (BT-Ba20), reducing network connectivity as shown in Table 1 and Figure 1. The increase in the molar volume confirms the structural role of BaO as a network modifier, creating Non-Bridging Oxygen (NBO) units.

Table 1: Density, molar volume (V_m), and the chemical constituents of the prepared glasses.

Sample codes	B_2O_3	TeO_2	Bi_2O_3	SrO	ZnO	BaO	Density (gcm^{-3})	Volume (cm^{3}mol^{-1})
BT-Ba5	65	10	10	5	5	5	4.028	32.840
BT-Ba10	60	10	10	5	5	10	4.102	33.026
BT-Ba15	55	10	10	5	5	15	4.736	36.913

BT-Ba20	50	10	10	5	5	20	4.813	37.063

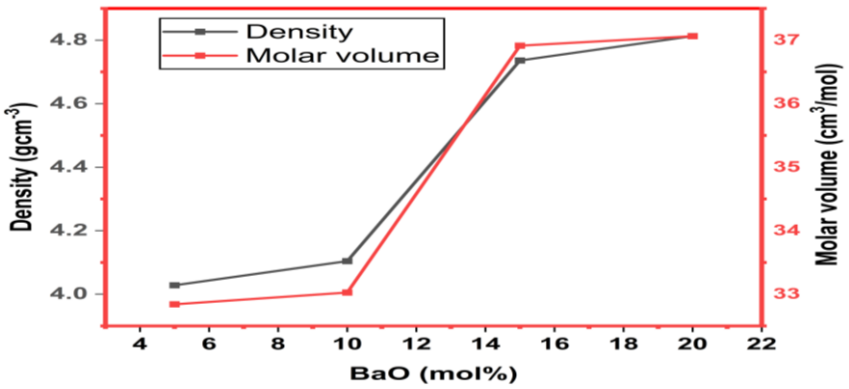


Figure 1: Density and molar volume against BaO content

The oxygen molar volume and oxygen packing density as shown in Table 2 and Figure 3 demonstrate opposite trends with oxygen molar volume increasing from 13.142 for BT-Ba5 to 13.405 cm^3mol^{-1} for BT-Ba20 while the oxygen packing density (OPD), decreases from 83.421 to 81.016 g.atm/l for the same glasses, due to increase in BaO concentrations, indicating expansion in the glass network and reduce the glass's compactness by reducing the packing efficiency of oxygen atoms. These properties are attributed to the modifier properties of BaO addition, disrupting the borate network through NBO formation. The Ba^{2+}concentrations increased from 15.5404×10^{19} ions cm^{-3} to 77.9800×10^{19} ions cm^{-3} for BT-Ba5 and BT-Ba20 glasses as it replaces B_2O_3, demonstrating a higher probability of photon interactions. Hence, increasing radiation attenuation properties. The polaron radius and inter-nuclear distance both decrease from 9.45 to 5.53 Å and from 23.448 to 13.713 Å, as shown in Figure 2, indicating an increase in Ba^{2+} forms localization of charges necessary for enhanced interactions between the neighboring modifier ions. The field strength increased from 0.7615×10^{16} to 2.4226×10^{16} cm^{-3} for BT-Ba5 and BT-Ba20 glasses, respectively. The higher field strength indicates increased electrostatic interaction between Ba^{2+} and the oxygen atom, influencing optical, structural stability, and radiation absorption properties of the glasses.

Table 2: Physical and optical properties of the prepared glasses

Physical parameters	**BT-Ba5**	**BT-Ba10**	**BT-Ba15**	**BT-Ba20**
Oxygen packing density (g atm/l)	83.421	82.831	82.542	81.016
Oxygen molar volume (cm^3/mol)	13.142	13.243	13.261	13.405
Ba^{2+} concentration ($\times 10^{19}$ ions cm^{-3})	15.5404	28.1249	38.9872	77.9800
Polaron radius, r_p (Å)	9.4500	7.5096	6.1624	5.5268
Inter-nuclear distance, r_i (Å)	23.448	18.6331	15.2904	13.7134
Field strength ($\times 10^{16}$ cm^{-3})	0.7615	1.3122	1.9487	2.4226
Direct energy band gap $E_{g(d)}$ (eV)	3.221	3.248	3.124	2.793
Indirect band gap energy $E_{g(in)}$ (eV)	3.016	3.143	3.055	2.847
Refractive index n	2.393	2.360	2.382	2.440
Reflection losses (R_L) %	28.590	28.663	32.103	32.403
Dielectric constant (ε)	5.726	5.570	5.674	5.954

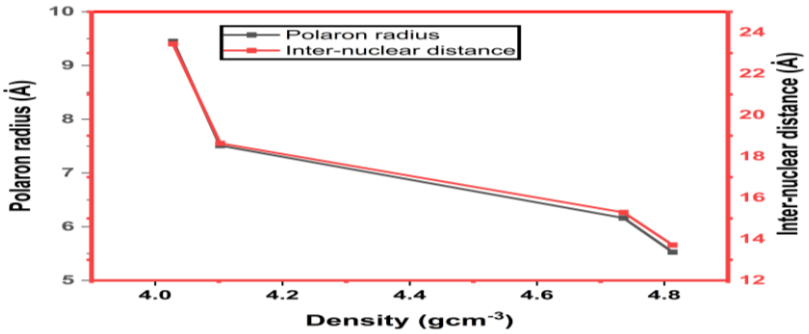


Figure 2: Variation of polaron radius and inter-nuclear distance against their densities

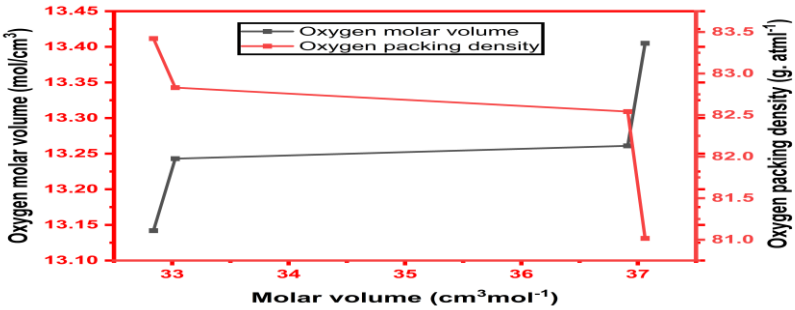


Figure 3: Variation of oxygen molar volume and oxygen packing density against molar volume.

Optical features of the prepared glass system

To investigate the optical transition characteristics of the glass samples, their optical absorption behavior was analyzed. Figure 4 presents the UV–Vis–NIR absorption spectra of BTBa glasses with different BaO concentrations over 200–2000 nm.

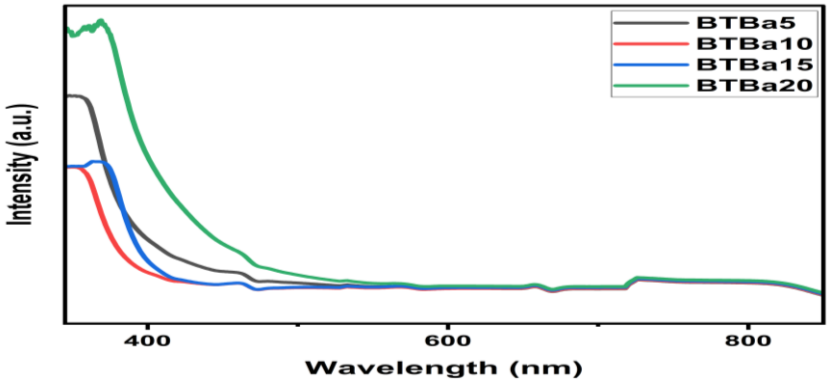


Figure 4: UV–Visible–NIR optical absorbance spectra of the BTBa glass samples.

For amorphous glass materials, the optical band gap can be determined by considering the nature of the electronic transition. Assuming an indirect allowed transition (m = 1/2), the optical band gap (E_g) was evaluated by plotting ($\alpha h\nu$) against photon energy ($h\nu$), following the Tauc method (Sayyed et al., 2023). Figure 5 shows the corresponding Tauc plots for indirect-allowed transition, while Figure 6 shows how the derived E_g values vary with BaO concentration for the BTBa glass samples. The measured E_g values are 3.016, 3.143, 3.055, and 2.847 eV for BTBa5, BTBa10, BTBa15, and BTBa20, respectively (see Table 2). The results reveal a non-monotonic dependence of E_g on BaO content, with an initial increase from 3.016 eV for BTBa5 to 3.143 eV for BTBa10, followed by a decrease to 3.055 and 2.847 eV for BTBa15 and BTBa20, respectively. The initial increase in E_g may be associated with a reduction in the concentration of non-bridging oxygen (NBO) sites within the glass network (Alrowaily et al., 2026).

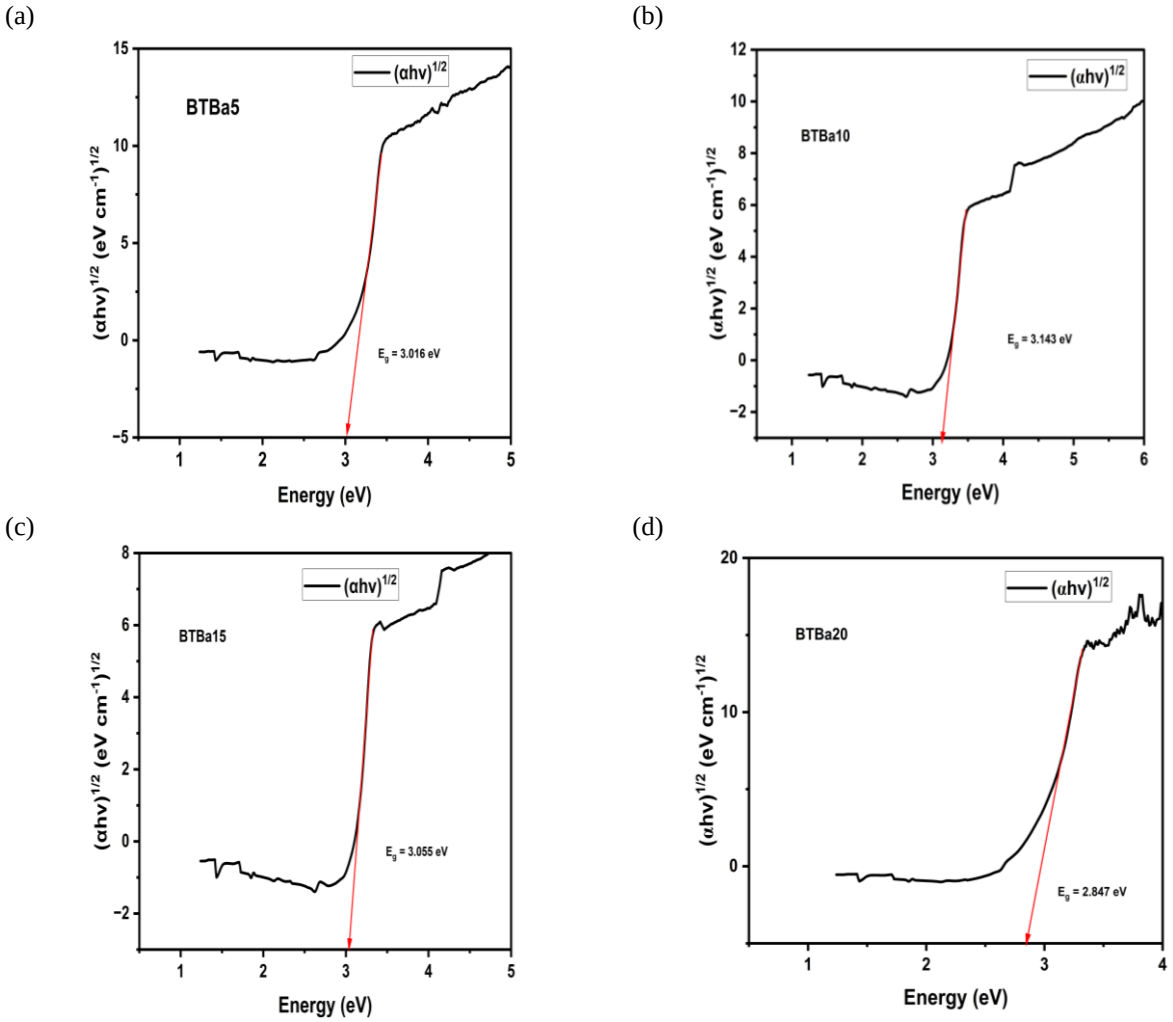


Figure 5: Tauc's plot for indirect- allowed transition against hν for all BTBa-glass samples.

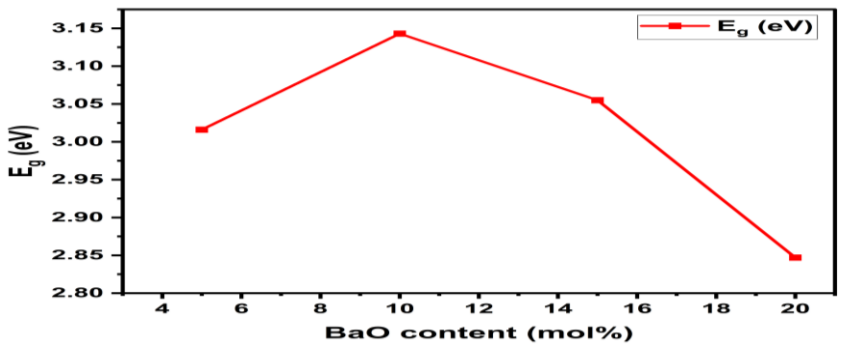


Figure 6: Variation of indirect energy band gap against BaO content for all BTBa-glass samples.

The refractive index and related optical parameters, including the dielectric constant and molar refraction, are summarized in Table 2. All three parameters exhibit a systematic increase with increasing BaO concentration, indicating a strong compositional dependence of the optical response of the glass network. The refractive index increases progressively with BaO content, which can be attributed to the increased polarizability and structural compactness associated with the incorporation of BaO into the glass matrix (Sayyed et al., 2023). The corresponding increase in dielectric constant is consistent with the higher electronic

polarizability of the modified glass network. Similarly, the variation in molar refraction reflects changes in the polarizability and local structural environment induced by BaO incorporation (Alrowaily et al., 2026). These trends collectively demonstrate that increasing BaO content modifies the structural compactness and polarizability of the glass network, thereby influencing its optical characteristics.

Gamma ray attenuation features

The linear attenuation coefficients (LAC) of the fabricated glass samples were determined experimentally over the investigated gamma-ray energy range. To verify the reliability and accuracy of the experimental measurements, we compared the measured LAC values with the corresponding theoretical values calculated using the Phy-X/PSD software. The comparison demonstrates good agreement between the experimental and theoretical results, thereby confirming the validity of the adopted experimental methodology and the accuracy of the attenuation measurements. Figure 7, which depicts measured LAC values for the BaO-based glass samples, shows good agreement with the corresponding Phy-X/PSD results, with the differences remaining within the acceptable limits of experimental uncertainty. The LAC values increased progressively with BaO concentration across the investigated energy range of 0.059-1.333 MeV, indicating that BaO incorporation enhances the gamma-ray attenuation capability of the glass matrix. At 0.059 MeV, all samples exhibited their highest LAC values, ranging from 12.474 cm^{-1} for BT-Ba5 to 18.432 cm^{-1} for BT-Ba20. The pronounced attenuation at this low energy is attributed to the dominance of the photoelectric absorption process, which is highly dependent on the effective atomic number and density of the shielding material (Al-Hadeethi & Sayyed, 2020). As the photon energy increased to 0.1 MeV, the LAC values decreased rapidly for all glass compositions owing to the diminishing contribution of the photoelectric effect and the increasing dominance of Compton scattering in the intermediate-energy region. Beyond this region, the LAC values declined more gradually as photon energy increased. At the highest investigated energy (1.333 MeV), the LAC values approached nearly constant values, reflecting the increasing contribution of pair production at high photon energies. Although pair production is possible at 1.333 MeV, its contribution remains limited by the relatively small excess energy (0.311 MeV) above the 1.022 MeV threshold. At this energy, the LAC values reached their minimum, varying from 0.218 cm^{-1} for BT-Ba5 to 0.257 cm^{-1} for BT-Ba20. Overall, the results demonstrate that increasing the BaO content will enhance the effective atomic number in the glass network, thereby significantly improving the gamma-ray shielding performance of the boro-tellurite glass system. Among the investigated compositions, BT–Ba20 exhibited the highest LAC values across the entire energy range, confirming its superior attenuation efficiency, whereas BT-Ba5 consistently showed the lowest LAC values.

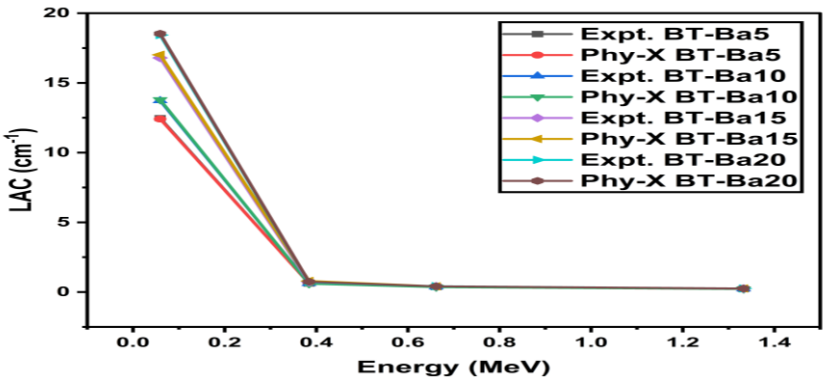


Figure 7: Measured LAC compared with Phy-X data for BT-Ba glasses.

The LAC values of the fabricated BT–Ba glasses were compared with those of commercially available SCHOTT radiation shielding glasses (RS-253, RS-253-G18, RS-360, and RS-520) (Alqahtani et al., 2022) over the photon energy range of 0.2-1.25 MeV, as illustrated in Figure 8. Among the samples investigated, BT-Ba20 exhibited the highest LAC values 2.118-0.263 cm^{-1}, surpassing those of RS-253 (0.320-0.140 cm^{-1}) and approaching the attenuation performance of RS-360 (1.720-0.210 cm^{-1}). Conversely, the LAC values of BT–Ba5 remained lower than those of RS-520 (3.540-0.300 cm^{-1}) throughout the investigated energy range. The superior attenuation performance of RS-520 is primarily attributed to its high PbO content (≈70 wt%) and higher density (5.2 g. cm^{-3}). In contrast, BT-Ba20 contains 20 mol% BaO and has a density of (4.813 g. cm^{-3}). Despite its lower density and lead-free composition, BT-Ba20 demonstrated attenuation characteristics comparable to

RS-360, indicating its potential as an environmentally friendly radiation shielding glass.

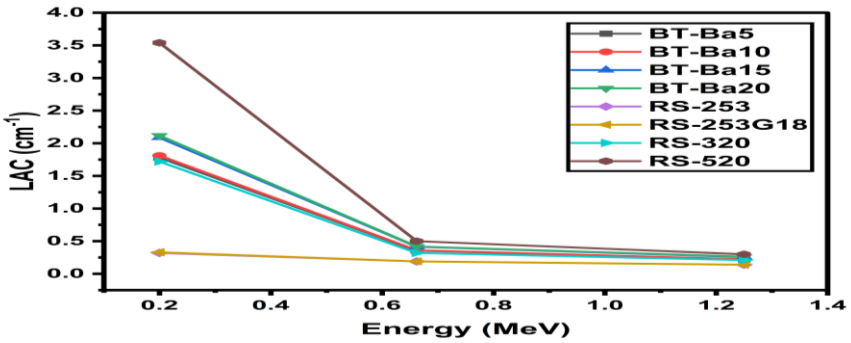


Figure 8: Comparison between measured LAC prepared and SCHOTT glasses

The half-value layer (HVL) of the barium-doped boro-tellurite glass samples was determined from the experimentally measured linear attenuation coefficient (LAC) values over the photon energy range of 0.059-1.333 MeV. As illustrated in Figure 9, the HVL values were lowest at 0.059 MeV, ranging from 0.038 cm for BT-Ba20 to 0.056 cm for BT-Ba5. The reduced HVL at this energy indicates the superior attenuation capability of the glass samples against low-energy gamma photons. As photon energy increased from 0.059 to 0.6616 MeV, the HVL values increased markedly for all glass compositions. This trend is attributed to the decreasing contribution of the photoelectric absorption process, whose interaction probability decreases rapidly with increasing photon energy, resulting in a greater material thickness being required to reduce the incident gamma-ray intensity by half. Beyond 0.059 MeV, the HVL values increased progressively with increasing photon energy for all investigated glass compositions. This behaviour is primarily attributed to the dominance of Compton scattering in the intermediate-energy region, where the interaction probability decreases with increasing photon energy, thereby requiring a greater material thickness to attenuate the incident gamma-ray intensity by 50%. At higher photon energy, the rate of increase in HVL became less pronounced, and the values approached an approximately constant trend as pair production gradually became a significant interaction mechanism. At the maximum investigated energy of 1.333 MeV, the HVL values reached their highest values, ranging from 3.180 cm for BT-Ba5 to 2.697 cm for BT-Ba20. The consistently lower HVL values exhibited by BT-Ba20 indicate its superior gamma-ray shielding efficiency, as a smaller thickness is required to achieve the same level of radiation attenuation compared with the other glass compositions.

Figure 10 compares the half-value layer (HVL) of the fabricated barium-doped boro-tellurite glasses with those of commercially available SCHOTT radiation shielding glasses (RS-253, RS-253-G18, RS-360, and RS-520) over the photon energy range of 0.2–1.25 MeV. Among the commercial glasses, RS-520 exhibited the lowest HVL values (0.196–2.310 cm), reflecting its superior shielding efficiency. Nevertheless, the fabricated BT–Ba glasses consistently showed lower HVL values than RS-253 and RS-253-G18 across the investigated energy range. In contrast, RS-253 recorded the highest HVL values, ranging from 2.166 to 4.951 cm, indicating the least effective attenuation performance among the commercial glasses considered. These results demonstrate that increasing the BaO content significantly enhances the shielding performance of the fabricated glasses, with BT–Ba20 exhibiting HVL values comparable to those of RS-360.

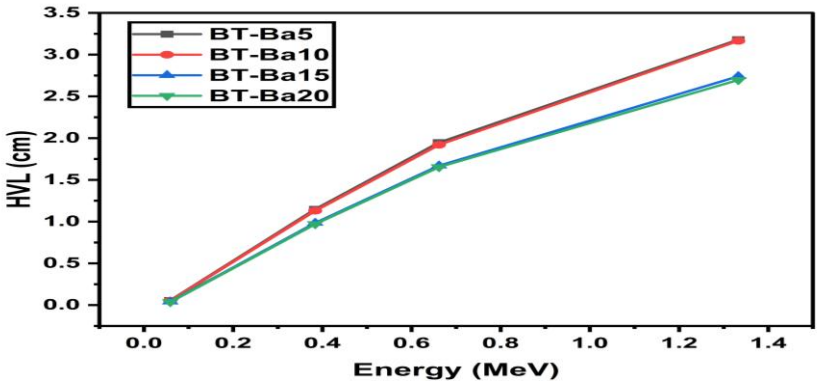


Figure 9: HVL of the prepared barium-activated boro-tellurite glasses

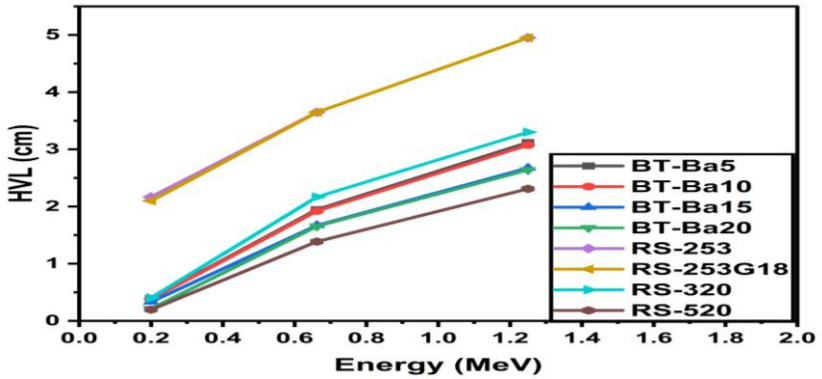


Figure 10: Comparison between HVL prepared and SCHOTT glasses

Figure 11 illustrates the variation of the effective atomic number Z_{eff} of the fabricated glass samples as a function of gamma-ray photon energy. The Z_{eff} values attained their maximum at 0.059 MeV, ranging from 52.19 for BT-Ba5 to 53.28 for BT-Ba20. Beyond this energy, a sharp decline in Z_{eff} was observed for all glass compositions with increasing photon energy. This behavior is primarily attributed to the dominance of the photoelectric absorption process, whose interaction cross-section is approximately proportional to $E^{-3.5}$ (Saudi & Abd-Allah, 2021). In the intermediate energy region (above 0.1 MeV), where Compton scattering becomes the prevailing interaction mechanism, Z_{eff} decreased progressively with increasing photon energy. At higher photon energy (above several MeV), Z_{eff} exhibited a gradual increase owing to the onset of pair production, whose cross-section varies approximately with log(E) (Iliyasu et al., 2023). The minimum Z_{eff} values were recorded around 1.333 MeV, ranging from 1.34 for BT-Ba5 to 1.51 for BT-Ba20. Furthermore, Figure 11, also presents the dependence of Z_{eff} on BaO concentration at different photon energies, demonstrating that increasing the BaO content consistently enhanced the effective atomic number of fabricated glasses across the investigated energy range. This improvement is attributed to the incorporation of barium, a high atomic number element, which increases the overall photon interaction probability and consequently enhances the radiation shielding capability of the glass system.

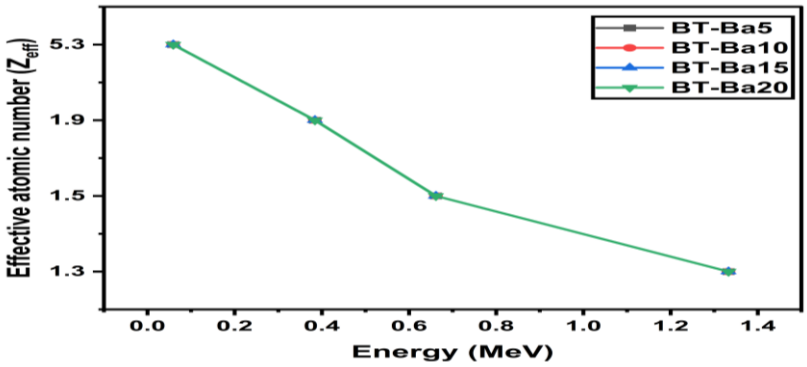


Figure 11: Variation of Z_{eff} of the fabricated glass samples against gamma energy

Mean free path (MFP) is an important parameter for evaluating the gamma-ray shielding effectiveness of materials, with lower MFP values indicating superior attenuation performance and reduced thickness requirements. Figure 12 illustrates the variation of the MFP for BT-Ba5, BT-Ba10, BT-Ba15, and BT-Ba20 glasses over the photon energy range of 0.059–1.333 MeV. For all compositions, the MFP increased with increasing photon energy, indicating that thicker glass samples are required to attenuate higher-energy gamma rays. For instance, the MFP of BT-Ba20 increased from 2.399 cm at 0.6616 MeV to 3.919 cm at 1.333 MeV. This trend is consistent with the dominant photon interaction mechanisms, namely photoelectric absorption at low energies, Compton scattering at intermediate energies, and pair production at high energies. Moreover, the MFP decreased progressively as BaO content increased, reflecting the enhanced shielding

capability of the fabricated glasses. Among all the samples investigated, BT-Ba20 exhibited the lowest MFP values, indicating that it requires the least thickness to achieve effective gamma-ray attenuation.

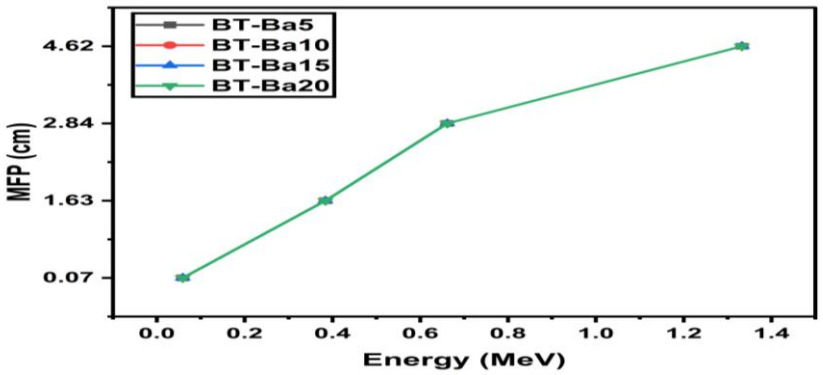


Figure 12: Variation of MFP of the fabricated glass samples against gamma energy.

CONCLUSION

Bismuth–strontium–zinc–telluro-borate glasses activated with BaO were successfully synthesized via the melt-quenching method and systematically characterized. The resulting glasses exhibited high optical transparency, confirming their suitability for potential optical and radiation-shielding applications. The incorporation of BaO led to an increase in glass density from 4.028 to 4.813 g cm^{-3}, accompanied by an increase in molar volume from 32.840 to 37.063 cm^3 mol^{-1}. In contrast, the oxygen packing density (OPD) decreased from 83.421 to 81.016 g atom l^{-1}, whereas the oxygen molar volume (OMV) increased slightly from 13.142 to 13.405 mol cm^{-3} with increasing BaO content. Optical analysis revealed that the optical band gap initially increased from 3.016 to 3.143 eV, followed by a decrease from 3.055 to 2.847 eV with increasing BaO content from 5 to 20 mol%. The initial increase in band gap is attributed to a reduction in the concentration of non-bridging oxygen (NBO) species within the glass network, which enhances network connectivity and reduces localized defect states. Furthermore, the radiation-shielding results demonstrated that the incorporation of BaO effectively enhanced the photon attenuation capability of the glasses. To further assess their radiation-protection performance, the half-value layer (HVL) values of the prepared glasses were compared with those of previously reported commercial shielding glasses at a photon energy of 0.059 MeV. The HVL values decreased from 0.056 cm for BT-Ba5 to 0.038 cm for BT-Ba20, indicating improved shielding performance with increasing BaO content. These HVL values were lower than those reported for RS-253 and RS-253G18, although they remained higher than those of RS-360 at the same photon energy. Overall, the results demonstrate that BaO incorporation is an effective strategy for enhancing the radiation-shielding performance of bismuth–strontium–zinc–telluro borate glasses. The results demonstrate that BaO is an effective modifier for tailoring the density, optical properties, and photon attenuation performance of Bi-containing boro-tellurite glasses. Further studies involving experimental mechanical testing, transmission measurements, chemical durability assessments, and Monte Carlo simulations are recommended to validate the glass material properties.

Acknowledgement

We are truly grateful for the financial support from TETFund Nigeria (Institution-Based Research, IBR). We also extend our gratitude to Federal University Gashua, Yobe State, for its invaluable assistance.

Data availability

The data supporting the findings of this study are available on request from the corresponding author.

REFERENCES

Abdullah, M. A. H., Rashid, R. S. M., Amran, M., Hejazii, F., Azreen, N. M., Fediuk, R., Voo, Y. L., Vatin, N. I., & Idris, M. I. (2022). Recent trends in advanced radiation shielding concrete for construction of facilities: materials and properties. *Polymers*, *14*(14), 2830.

Abdullahi, I., Hashim, S., Ghoshal, S. K., Sayyed, M. I., & Thabit, H. A. (2024). Significant greenish–yellow emission from Dy3+/Sm3+ co-doped strontium–aluminate–telluro-borate glasses: role of Ag and CuO nanoparticles interplay. *Journal of Materials Science*, 1–19.

AbuAlRoos, N. J., Amin, N. A. B., & Zainon, R. (2019). Conventional and new lead-free radiation shielding materials for radiation protection in nuclear medicine: A review. *Radiation Physics and Chemistry*, *165*, 108439.

Al-Buriahi, M. S., Singh, V. P., Alalawi, A., Sriwunkum, C., & Tonguc, B. T. (2020). Mechanical features and radiation shielding properties of TeO2–Ag2O-WO3 glasses. *Ceramics International*, *46*(10), 15464–15472. https://doi.org/10.1016/j.ceramint.2020.03.091

Al-Hadeethi, Y., & Sayyed, M. I. (2020). A comprehensive study on the effect of TeO2 on the radiation shielding properties of TeO2–B2O3–Bi2O3–LiF–SrCl2 glass system using Phy-X / PSD software. *Ceramics International*, *46*(5), 6136–6140. https://doi.org/https://doi.org/10.1016/j.ceramint.2019.11.078

Al-Harbi, N., Sayyed, M. I., Al-Hadeethi, Y., Kumar, A., Elsafi, M., Mahmoud, K. A., Khandaker, M. U., & Bradley, D. A. (2021). A novel CaO–K2O–Na2O–P2O5 glass systems for radiation shielding applications. *Radiation Physics and Chemistry*, *188*, 109645. https://doi.org/https://doi.org/10.1016/j.radphyschem.2021.109645

Alazoumi, S. H., Aziz, S. A., El-Mallawany, R., Aliyu, U. S., Kamari, H. M., Zaid, M. H. M. M., Matori, K. A., & Ushah, A. (2018). Optical properties of zinc lead tellurite glasses. *Results in Physics*, *9*, 1371–1376. https://doi.org/https://doi.org/10.1016/j.rinp.2018.04.041

Alomairy, S., Alrowaili, Z. A., Kebaili, I., Wahab, E. A. A., Mutuwong, C., Al-Buriahi, M. S., & Shaaban, K. S. (2022). Synthesis of Pb3O4-SiO2-ZnO-WO3 Glasses and their Fundamental Properties for Gamma Shielding Applications. *Silicon*, *14*(10), 5661–5671. https://doi.org/10.1007/s12633-021-01347-2

Alonizan, N., Hamad, M. K., Alwabsi, A., Dwaikat, N., Mhareb, M. H. A., Sayyed, M. I., Thabit, H. A., Alajerami, Y. S., & Makhadmeh, G. N. (2023a). Physical, optical, and ionizing radiation shielding properties for barium–tellurite glass with different oxides: An experimental study. *Optical Materials*, *143*, 114177. https://doi.org/https://doi.org/10.1016/j.optmat.2023.114177

Alonizan, N., Hamad, M. K., Alwabsi, A., Dwaikat, N., Mhareb, M. H. A., Sayyed, M. I., Thabit, H. A., Alajerami, Y. S., & Makhadmeh, G. N. (2023b). Physical, optical, and ionizing radiation shielding properties for bariumâ€“tellurite glass with different oxides: An experimental study. *Optical Materials*, *143*. https://doi.org/10.1016/j.optmat.2023.114177

Aloraini, D. A., Almuqrin, A. H., Sayyed, M. I., Kumar, A., Gaikwad, D. K., Tishkevich, D. I., & Trukhanov, A. V. (2021). Experimental and theoretical analysis of radiation shielding properties of strontium-borate-tellurite glasses. *Optical Materials*, *121*, 111589. https://doi.org/https://doi.org/10.1016/j.optmat.2021.111589

Alqahtani, M. S., Hussein, K. I., Afifi, H., Reben, M., Grelowska, I., Zahran, H. Y., Yahia, I. S., & Yousef, E. S. (2022). Optical and radiation shielding characteristics of tellurite glass doped with different rare-earth oxides. *Journal of X-Ray Science and Technology*, *30*(2), 293–305. https://doi.org/10.3233/XST-211017

Alrowaily, A. W., Kumar, A., Ngaram, S. M., & Sayyed, M. I. (2026). Impact of BaO Concentration on the Structural, Mechanical, Optical, and Gamma-Ray Shielding Competence of B2O3-Na2O-Al2O3-CaO Glasses. *Radiation Physics and Chemistry*, 114109.

Alzahrani, J. S., Eke, C., Alrowaili, Z. A., Somaily, H. H., Sriwunkum, C., & Al-Buriahi, M. S. (2022). Evaluation of the radiation shielding characteristics of WO3–MoO3–TeO2/Sb2O3 glasses. *Canadian Metallurgical Quarterly*, *61*(4), 418–428. https://doi.org/10.1080/00084433.2022.2058153

Aniebone, V. O., & Gafar, A. I. A. A. (2023). Radiation exposure and health effects on the human body. *Journal of Computational Mechanics*, *6*(3).

Ardiansyah, A., Heryanto, H., Armynah, B., Salah, H., Sulieman, A., Bradley, D. A., & Tahir, D. (2023). Physical, mechanical, optical, and gamma radiation shielding properties of the BaO-based glass system prepared by the melt-quench technique: A review. *Radiation Physics and Chemistry*, *210*, 111059. https://doi.org/10.1016/J.RADPHYSCHEM.2023.111059

Atta, M. M., Abou-Laila, M. T., Abdelwahed, M. H., Dwidar, S. A., & Desouky, O. (2023). Structural, mechanical, and thermal features of PVA/starch/graphene oxide nanocomposite enriched with WO3 as gamma–ray radiation shielding materials for medical applications. *Polymer Engineering and Science*. https://doi.org/10.1002/pen.26490

Bakri, F., Gareso, P. L., & Tahir, D. (2024). Advancing radiation shielding: A review the role of Bismuth in X-ray protection. *Radiation Physics and Chemistry*, 111510.

Barbhuiya, S., Das, B. B., Norman, P., & Qureshi, T. (2025). A comprehensive review of radiation shielding

concrete: Properties, design, evaluation, and applications. *Structural Concrete*, *26*(2), 1809–1855.

Boonin, K., Yasaka, P., Limkitjaroenporn, P., Rajaramakrishna, R., Askin, A., Sayyed, M. I., Kothan, S., & Kaewkhao, J. (2020). Effect of BaO on lead free zinc barium tellurite glass for radiation shielding materials in nuclear application. *Journal of Non-Crystalline Solids*, *550*. https://doi.org/10.1016/j.jnoncrysol.2020.120386

Bozkurt, M., Şahin, N., Karabul, Y., Kılıç, M., & Özdemir, Z. G. (2022). Radiation shielding performances of Na2SiO3 based low-cost micro and nano composites for diagnostic imaging. *Progress in Nuclear Energy*, *143*. https://doi.org/10.1016/j.pnucene.2021.104058

Dimitrov, V., & Komatsu, T. (2010). An interpretation of optical properties of oxides and oxide glasses in terms of the electronic ion polarizability and average single bond strength. *J. Univ. Chem. Technol. Metall*, *45*(3), 219–250.

Harrington, K. J. (2016). The biology of cancer. *Medicine*, *44*(1), 1–5.

Iliyasu, U., Mohd Sanusi, M. S., & Ahmad, N. E. (2023). The effect of WO3 on the optical and radiation shielding properties of zinc-lead-borate glass. *Radiation Physics and Chemistry*, *209*(April), 111007. https://doi.org/10.1016/j.radphyschem.2023.111007

Iliyasu, U., Mohd Sanusi, M. S., Ahmad, N. E., Al-Buriahi, M. S., Thabit, H. A., Bature, M., & Modu, N. S. (2025). Fabrication of Cd-modified Zn-Pb-W-borate glass for enhanced optical, thermal, and radiation attenuation. *Solid State Sciences*, *160*, 107797. https://doi.org/https://doi.org/10.1016/j.solidstatesciences.2024.107797

Issa, S. A. M., Tekin, H. O., Saudi, H. A., Koubisy, M. S. I., Zhukovsky, M., Ali, A. S., & Zakaly, H. M. H. (2022). Fabrication of newly developed tungsten III-oxide glass family: Physical, structural, mechanical, radiation shielding effectiveness. *Optik*, *259*. https://doi.org/10.1016/j.ijleo.2022.169025

Jahng, J. W. S., Little, M. P., No, H. J., Loo Jr, B. W., & Wu, J. C. (2024). Consequences of ionizing radiation exposure to the cardiovascular system. *Nature Reviews Cardiology*, *21*(12), 880–898.

Knoll, G. F. (2010). *Radiation detection and measurement*. John Wiley & Sons.

Kozlovskiy, A. L., Shlimas, D. I., Zdorovets, M. V, Elsts, E., Konuhova, M., & Popov, A. I. (2023). Investigation of the Effect of PbO Doping on Telluride Glass Ceramics as a Potential Material for Gamma Radiation Shielding. *Materials*, *16*(6). https://doi.org/10.3390/ma16062366

Kozlovskiy, A., Zdorovets, M. V, & Kadyrzhanov, K. K. (2021). Study of physical, optical properties and gamma radiation shielding efficiency of 0.5Bi2O3-(0.5-x)WO3-xPbO glasses. *Optical Materials*, *114*. https://doi.org/10.1016/j.optmat.2021.111005

Mhareb, M. H. A., Alajerami, Y. S. M., Sayyed, M. I., Dwaikat, N., Alqahtani, M., Alshahri, F., Saleh, N., Alonizan, N., Ghrib, T., & Al-Dhafar, S. I. (2020). Radiation shielding, structural, physical, and optical properties for a series of borosilicate glass. *Journal of Non-Crystalline Solids*, *550*, 120360. https://doi.org/https://doi.org/10.1016/j.jnoncrysol.2020.120360

Mhareb, M. H. A., Sayyed, M. I., Mahdi, R. I., Kaky, K. M., Hamad, M. K., & Kadhim, A. J. (2025). Role of Nd (III) ions on B2O3–TeO2-GeO2-MgO glass composition for optical and ionizing protection application. *Nuclear Engineering and Technology*, *57*(1), 103162. https://doi.org/https://doi.org/10.1016/j.net.2024.08.031

Ngaram, S. M., Hashim, S., Sanusi, M. S. M., Abdullahi, I., & Sayyed, M. I. (2025). Experimental evaluation of tungsten-doped boro-tellurite glasses for structural and improved radiation shielding properties. *Journal of Materials Science: Materials in Electronics*, *36*(21), 1–14.

Ngaram, S. M., Hashim, S., Sanusi, M. S. M., & Ibrahim, A. (2025). Enhanced physical, optical and radiation shielding properties of tungsten modified potassium boro-tellurite glass systems: Theoretical approach. *Radiation Physics and Chemistry*, *226*, 112355. https://doi.org/https://doi.org/10.1016/j.radphyschem.2024.112355

Ngaram, S. M., Hashim, S., Sanusi, M. S. M., Ibrahim, A., & Sayyed, M. I. (2024). Structural and optical characteristics of B2O3-TeO2-Bi2O3-SrCO3-K2CO3-Er2O3 glass systems: Role of Er3+ doping. *Ceramics International*. https://doi.org/https://doi.org/10.1016/j.ceramint.2024.12.033

Qazi, U. Y. (2022). Future of hydrogen as an alternative fuel for next-generation industrial applications;

challenges and expected opportunities. *Energies*, *15*(13), 4741.

Sathiyapriya, G., Marimuthu, K., Sayyed, M. I., Askin, A., & Agar, O. (2019). An investigation on physical, structural and gamma ray shielding features of Dy3+ ions doped Telluroborate glasses. *Journal of Non-Crystalline Solids*, *522*, 119574. https://doi.org/https://doi.org/10.1016/j.jnoncrysol.2019.119574

Saudi, H. A., & Abd-Allah, W. M. (2021). Structural, physical and radiation attenuation properties of tungsten doped zinc borate glasses. *Journal of Alloys and Compounds*, *860*. https://doi.org/10.1016/j.jallcom.2020.158225

Sayyed, M. I., El-bashir, B. O., Alhuthali, A. M. S., Alajerami, Y. S. M., Al-Hadeethi, Y., & Mhareb, M. H. A. (2021). Gamma radiation shielding and structural features for barium strontium boro-tellurite glass modified with various concentrations of molybdenum oxide. *Journal of Non-Crystalline Solids*, *559*, 120658. https://doi.org/https://doi.org/10.1016/j.jnoncrysol.2021.120658

Sayyed, M. I., Morshidy, H. Y., Shaaban, K. S., Abd El-Rehim, A. F., Ali, A. M., & Sadeq, M. S. (2023). Impacts of BaO additions on structure, linear/nonlinear optical properties and radiation shielding competence of BaO–NiO–ZnO–B2O3 glasses. *Optical Materials*, *144*, 114300.

Sonia, Y. K., & Meena, S. (2024). Eco-materials: opportunity, applications, and challenges. *Eco-Materials and Green Energy for a Sustainable Future*, 75–92.

Talapko, J., Talapko, D., Katalinić, D., Kotris, I., Erić, I., Belić, D., Vasilj Mihaljević, M., Vasilj, A., Erić, S., & Flam, J. (2024). Health effects of ionizing radiation on the human body. *Medicina*, *60*(4), 653.

Usman, A., M.K., H., Latif, A. A., Muhammad, F. D., & Abubakar, A. I. (2018). Influence of Ho3+ ions on structural and optical properties of zinc borotellurite glass system. *Journal of Non-Crystalline Solids*, *483*, 18–25. https://doi.org/https://doi.org/10.1016/j.jnoncrysol.2017.12.040

Usman, I., Sanusi, M. S. M., Ahmad, N. E., & bin Shaharin, M. S. (2023). Structural and optical properties of tungsten-sodium-zinc-borate glass doped α-Fe2O3 nanoparticle. *Ceramics International*, *49*(16), 26256–26266.

Wang, B., Qiu, T., Yuan, L., Fang, Q., Wang, X., Guo, X., Zhang, D., Lai, C., Wang, Q., & Liu, Y. (2023). A comparative study between pure bismuth/tungsten and the bismuth tungsten oxide for flexible shielding of gamma/X rays. *Radiation Physics and Chemistry*, *208*. https://doi.org/10.1016/j.radphyschem.2023.110906

Weeden, C. E., Hill, W., Lim, E. L., Grönroos, E., & Swanton, C. (2023). Impact of risk factors on early cancer evolution. *Cell*, *186*(8), 1541–1563.

Wu, Y., & Wang, Z. (2024). Progress in ionizing radiation shielding materials. *Advanced Engineering Materials*, *26*(21), 2400855.